J. Fluid Mech. (1995), *vol.* 285, *pp.* 17–40

Mixing due to grid-generated turbulence of a two-layer scalar profile

By PABLO HUQ[1] AND REX E. BRITTER[2]

[1] College of Marine Studies, University of Delaware, Newark, Delaware 19716, USA

[2] Department of Engineering, University of Cambridge, Cambridge CB2 1PZ, UK

(Received 25 October 1989 and in revised form 18 May 1994)

In this experimental study the mixing of passive scalars that arises from shear-free decaying grid-generated turbulence is examined. The flow configuration consists of two homogeneous layers of equal density separated by a sharp interface between different mean concentrations of passive scalar. Both layers flow through a turbulence-generating grid. To determine the effect of diffusivity the scalar was heat in one experiment and salt in a second. The Schmidt number – the ratio of momentum to species diffusivity – was 7 and 700 for heat and salt respectively. Velocity, scalar and flux fields were mapped and flow visualization was undertaken to study the flows.

Integral lengthscales and (scalar) flux were determined to be independent of diffusivity, whereas the scalar Taylor microscales varied with Schmidt number, S_c, thus illustrating the disparate effects of diffusivity on large and small scales. The time series of signals showed a correspondence between locations of $w\theta$ extrema and uw extrema. Flux $w\theta$ arose from intermittent events; and the magnitude of the time-averaged flux $\overline{w\theta}$ was found to depend on the frequency, rather than on variations in the amplitude of $w\theta$ events.

1. Introduction

There is a continuing need for better prediction of mixing rates. For example, knowledge of mixing rates is crucial in the chemical engineering industry to optimize yields from reacting chemicals. There is, however, a lack of understanding of the mechanisms of turbulent mixing. This is true even for the case of dynamically passive scalars. We consider here how passive scalars in shear-free decaying grid-generated turbulence are mixed between two homogeneous layers that have equal density but different initial scalar concentrations. Measurements are made of the evolution of the scalar flux $\overline{w\theta}$, the scalar variance $\overline{\theta^2}$, profiles of the mean scalar concentration C, and u and w, the horizontal and vertical components of the turbulent velocity field.

While the ultimate measure of mixing is the attainment of homogeneity at the molecular level, in turbulent flows the mean density, or concentration profile, tells little about the degree of molecular mixing. Turbulent mixing between two fluids with zero diffusivities would result in no mixing in the molecular sense, even though the mean profiles may be homogeneous. The two fluids would remain permanently separated by a highly convoluted interface. Accordingly, when turbulence is present in fluid flows, the stirring of the fluid and the final process of molecular mixing should be examined individually. In fluids with finite diffusivity, the processes of entrainment and molecular mixing occur simultaneously, though at disparate scales. Hence they are not easily distinguishable experimentally.

Brown & Roshko (1974) established the significance of large-scale structures arising

from the shear of a mixing layer in determining mixing rates. The purpose of this paper is to show that for shear-free decaying grid-generated turbulence, mixing rates are also controlled by large-scale structures, namely integral-scale eddies. We will show that the time-averaged flux $\overline{\theta w}$ is independent of molecular diffusivity for this flow. Furthermore, the flux is found to arise from intermittent events. Statistics of the mixing events show that the magnitude of the time-averaged flux depends on the frequency, rather than on variations in the amplitude of $w\theta$ events. The effect of molecular diffusion occurs at small scales, and this effect is shown by a dependence of the magnitude of the scalar fluctuations on the Schmidt number S_c. After reviewing relevant research on turbulence and mixing in §2, §3 will describe the experimental set-up and apparatus. Results and discussion are presented in §4, and, finally, the summary and conclusions follow in §5.

2. Previous work

A number of previous investigators have considered the problem of the turbulent mixing of passive scalars, both theoretically and experimentally. Corrsin (1951) considered the problem of turbulent transport in an isotropic homogeneous incompressible turbulent flow with a linear gradient of a passive scalar – with the understanding that the mean scalar gradient $\mathrm{d}T/\mathrm{d}Y$ is constant over a region very large compared with any dimension characterizing the fluctuating field. Using a Lagrangian diffusion analysis in the manner of Taylor (1921), but in reverse, Corrsin deduced that for a fluid with zero molecular diffusivity the scalar fluctuations $\overline{\theta^2}$ grow as $\overline{\theta^2} \sim x$ (for $t > T_L$, the Lagrangian integral timescale), and that the mean scalar profile stays linear. (Lin 1959 gave the physical explanation that the combination of homogeneity, isotropy and linear scalar profiles ensures that there is an equal likelihood of a particle arriving at a point with an excess or deficit of concentration, so that the mean profile stays linear.) For fluid with finite molecular diffusivity, assuming that equilibrium arises between production (with the gradient) and decay of $\overline{\theta^2}$, Corrsin further deduced that the scalar transport (i.e. normalized flux $\overline{\theta w}/\theta' w'$ where θ' and w' are the root-mean-square values of the variance of the scalar fluctuation $\overline{\theta^2}$ and the turbulent velocity fluctuation $\overline{w^2}$ respectively) would attain asymptotic values.

Despite the longitudinal inhomogeneity of the velocity field of laboratory grid-generated turbulence, Corrsin's predictions have been verified by Wiskind (1962), Alexopoulos & Keffer (1971), Venkataramani & Chevray (1978), and Sirivat & Warhaft (1983). These experiments, all conducted in wind tunnels, employed a transverse linear temperature gradient. The grid Reynolds number $R_M = \bar{U}M/v$ for these experiments was of order 10000, where $\bar{U}$ is the mean velocity, M is the spacing of the bars of the turbulence-generating grid, and v is the kinematic viscosity. The Prandtl number, P_r – the ratio of momentum to thermal diffusion – was equal to 0.7. For similar parameters, Budwig, Tavoularis & Corrsin (1985) utilized a streamwise linear gradient and also found that the linear gradient was preserved. For all cases asymptotic values (0.5–0.7) for the normalized flux ($\overline{\theta u_i}/\theta' u_i'$, no sum) parallel to the mean-scalar gradient were observed. The results of the above experiments vindicated Corrsin's analysis of the passive linear case: the effect of the longitudinal inhomogeneity of the velocity field was seemingly inconsequential, owing to the compensatory increase in integral length and time scales (Batchelor & Townsend 1956).

The present configuration of the stepwise profile of a passive scalar in shear-free decaying grid-generated turbulence (see figure 1) differs from the linear passive scalar gradient case in that additional transverse gradients contribute to the transport,

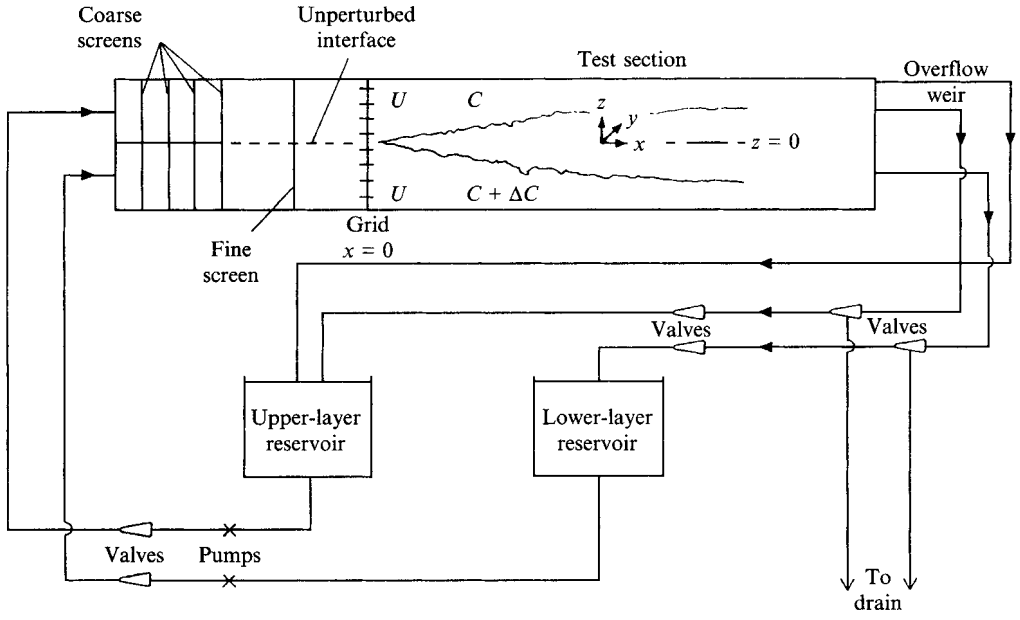

FIGURE 1. Schematic of experimental set-up and hydraulics. Also indicated is a right-handed coordinate system.

because the gradient of the mean concentration of passive scalar $\partial C/\partial z$ is not constant, unlike the case of the linear passive scalar gradient profile. Similarity analysis of the stepwise mean scalar profile (Libby 1975) showed that close to the grid temperature fluctuations were diffused across the mixing region, and that the production of temperature fluctuations by the gradient of mean temperature was relatively ineffective. For large distances, the fluctuations were determined by the gradient of mean temperature. In addition, he found that at the centreline of the mixing region the value of the maximum intensity of temperature fluctuation was constant.

As for linear gradient profiles of passive scalar, only wind tunnel experiments with temperature as the scalar (i.e. $R_M \sim 10000$, $P_r = 0.7$) have been done for the scalar profile of two homogeneous layers of equal density, but differing initial scalar concentrations. Watt & Baines (1973) found that the mean temperature profile evolved in a self-similar manner which was described by an error function profile. The development of the normalized turbulent transport ($\overline{\theta w}/\theta' w'$) and temperature fluctuation ($\theta'/\Delta T$) were also found to be described by error functions, though the agreement at the edges was less good. For turbulence generated by a mono-plane grid of horizontal bars, Keffer, Olsen & Kawall (1977) found the maximum value of temperature fluctuation to be constant for large distances. This finding implied that the flow had reached a state of equilibrium with production and diffusion balancing dissipation. Libby's (1975) analysis was in agreement with the wind-tunnel experiments of LaRue & Libby (1981) and LaRue, Libby & Seshadri (1981) but for the fact that the maximum temperature fluctuation predicted by Libby was considerably greater (predicted $\theta'/\Delta T \approx 0.31$ compared with the observed ~ 0.22). Though LaRue *et al.* (1981) accounted for this difference by adjusting the virtual origin, the discrepancy has not been satisfactorily explained. And, although the numerical studies of MacInnes (1985) and Jones & Musonge (1988) have reproduced the scalar evolution of LaRue *et al.* (1981), the modelling appears to be incomplete. Examination of the transport

equation for scalar fluctuations suggested that the evolution was dependent upon the ratio of molecular diffusivities, the Schmidt (or Prandtl) number. Experiments in this study were undertaken with Schmidt number values of 7 and 700, and comparison with wind tunnel results ($P_r = 0.7$) show that there was indeed a dependence of the evolution of the scalar fluctuations upon the Schmidt number.

3. Experimental set-up and apparatus

For the experiments a low background turbulence, two-layer recirculating water tunnel was designed and built: the tunnel, 15 cm wide, 20 cm deep and 225 cm long, was constructed from 1.27 cm thick Plexiglas. A free surface allowed the introduction of probes at any longitudinal section. Each layer was driven by a centrifugal pump, and the top water level was maintained by an overflow weir. A schematic of the experimental set-up and hydraulics is shown in figure 1 (and see Huq 1990 for more details).

First, the scalar was marked by adding brine ($S_c = 700$) to the lower-layer reservoir and by dissolving household sugar to the upper-layer reservoir until the densities matched. Next it was marked by a small temperature difference (~ 0.5 °C; $S_c = 7$), determined insufficient to be dynamically significant ($g' l_u^2/u'^2 < 1$ at the centre of the test section, where g' is the reduced gravitational acceleration and l_u the integral lengthscale derived from autocorrelation of the u-signal).

To ensure quiescent flow (prior to the introduction of the turbulence grid), mesh screens, coarse and fine, were used as turbulence suppressors; free-stream turbulence $w'/\bar{U}$ was measured to be 0.2% at the unperturbed interface. There was no measurable shear between the layers, and little interfacial mixing was observed. Turbulence was generated by a grid of bars comprising a square mesh of 3.2 cm spacing between bars of width $M = 0.64$ cm and thickness $d = 0.2$ cm (i.e. $M/d = 5$) so that the grid solidity was 36%. The value of the mean velocity, $\bar{U}$, was 7.7 cm s^{-1} for all the runs so that the grid Reynolds number ($R_M = \bar{U}M/\nu$) was approximately 2500. A typical value of the microscale Reynolds number $u'\lambda_g/\nu$ was 15 where λ_g is the Taylor microscale. Aside from the boundary layers arising from the sides, bottom and top surfaces (which grew to 2 cm at the location of the furthest downstream measurement point), the turbulence generated was measured to be vertically homogeneous to within 5% in the root-mean-square values for u and w at that location. This arrangement of pre-mixing – that is, the introduction of the scalars upstream of the grid – avoids complications when the origins of the turbulent velocity and scalar fields are not coincident (Warhaft & Lumley 1978).

The scalar difference between the layers eroded slowly over time owing to the closed-loop recirculation, and the time of reading was noted in order to make a (linear) correction. In addition, the experiments were performed after midnight, when ambient laboratory temperatures were dropping, in order to minimize temperature increase due to frictional heating. The temperature increase was 0.2 °C/hour, and over the duration of the experiment (typically less than half an hour) no temperature corrections for the probes were necessary. For salinity measurements, an aspirating conductivity probe with a 1 mm diameter sensor (2 mm long) and an end orifice of 0.33 mm (see Bidokhti & Britter 1987 for details) was operated in an AC bridge at 2 kHz. The frequency response was determined to be 70 Hz. The spatial resolution of the probe was estimated to be 0.4 mm, which, though less than the Kolmogorov length (defined by $l_{Kol} = (\nu^3/\epsilon)^{1/4} \approx 1$ mm over the length of the tunnel where ϵ is the energy dissipation rate), placed a stringent constraint on resolution of high wavenumbers ($k < 25$ cm^{-1}).

Constant-salinity baths up to four times the maximum concentration difference were used to calibrate the probe prior to each run; consequently temperature dependence was not a consideration. Calibration for these low concentrations were found to be linear and free of drift over the range used.

Temperature measurements were obtained with a quartz-coated hot film (Dantec probe 55R61-element of diameter 0.07 mm and length 1.25 mm, frequency response better than 100 Hz). This was operated as a 'cold-wire' resistance thermometer by a PSI Model 6100 anemometer used as a constant-current bridge. The wire heating at 4 mA was established to be sufficiently low that the parasitic influence of velocity fluctuations was negligible. Calibration of the cold wire was done in constant-temperature baths before each non-isothermal run.

Velocity measurements with hot films in aqueous flows are difficult to determine owing to bubble formation on the film surfaces, which occurs even when hot films are operated as low as 10 °C above the ambient fluid temperature. The low temperatures required to minimize 'bubbling' cause films to be highly sensitive to temperature changes from frictional heating, a phenomenon which is inevitable in recirculating systems. These problems, however, were overcome in the present experiments by de-aerating the water in the reservoirs, by waiting three days between runs, and by minimizing the frictional heating rate to 0.2 °C/hour.

Standard quartz-coated TSI cylindrical X-films (Type 1241-60w), with 0.15 mm diameter and 2.03 mm long sensors, were used for velocity measurements in conjunction with a second PSI Model 6100 anemometer operated with 4% overheat in constant-temperature mode. Prior to a run, the X-films were calibrated in a convergent nozzle over a range of velocities (4–12 cm s^{-1}) that were centred on the mean velocity ($\bar{U} = 7.7$ cm s^{-1}) used for the experiments. Measurements of w' were possible in the (weakly) non-isothermal environment of the heat experiments, because, as Bradshaw (1971) states, 'it is worth noting that (to first order) the difference between the outputs of two perfectly matched wires in an X-probe is independent of the temperature fluctuations: thus $\overline{v^2}$ or $\overline{w^2}$ can be measured as usual'. Indeed, measured values of w' and one-dimensional spectra for $S_c = 7$ and 700 were found to be indistinguishable. The small rate of frictional heating did not warrant temperature correction, however, because of the small length-to-diameter ratio (~ 15) yaw corrections with $k = 0.25$ (Champagne & Sleicher 1967; Lawson & Britter 1983). Errors in r.m.s. of the velocity fluctuations and correlation measurements were typically 5% and 10% respectively.

For flux measurements the 'cold wire' (or the aspirating conductivity probe) was used in combination with the X-film probe used for velocity measurements. The cold wire was located 1 mm from the X-probe, and the spatial resolution of the combined flux probe was estimated to be 1.5 mm (also the value for the combined flux probe comprising the aspirating conductivity probe). There was no discernible effect on the turbulent intensities arising from any distortion of the flow field, due to the presence of the conductivity probe or the cold wire. Furthermore, no cross-probe interference was observed in tests with permutations of probes being switched on or off.

Offset voltages from a programmable gain amplifier were added to the scalar and velocity signals before recording on FM tape to exploit the full input range (± 1 v) of a Racal Store 7 recorder. Signals were recorded at a tape speed of $3\frac{3}{4}$ in. s^{-1} so that the recording bandwidth was 0–1.25 kHz; it was subsequently digitized at 50 Hz, by a 12-bit analogue-digital interface driven by a microcomputer, and stored on flexible disks. Statistical analysis of the digitized data was obtained by appropriate standard software. Analysis of the θw signal was undertaken to examine burst activity with an

empirically determined threshold (that which least changed the total number of bursts) for each time series. Spectral analysis was done by a HP54410A/5420B signal analyser.

For flow visualization, fluorescein dye for laser-induced fluorescence (LIF) could be introduced to either reservoir without perceptibly changing the density. The test section was illuminated along the centreline (i.e. the x,z-plane) with a plane sheet of light ($\sim$ 1 mm in thickness – comparable with the Kolmogorov length) which was formed from an argon-ion laser (Lexel Model 95, operating at 2 W) by means of three 45° mirrors and a spherical and a cylindrical lens. Cross-sectional views of the (y,x)-plane at 25° to the mean flow direction were obtained by re-orienting the cylindrical lens.

4. Results and discussion

The following sections report quantitatively the measurements undertaken in the experiments. Observations from flow visualization are described in §4.1, and §§4.2 and 4.3 describe the turbulent velocity field and the self-similar mean scalar profiles. Next, in §4.4, details are given of lengthscales. They show the dependence of the small scales on, and the independence of the large scales of, the value of the Schmidt number S_c. The differing evolution of the scalar variance, and the different forms of scalar spectra for $S_c = 7$ and $S_c = 700$, are shown in §§4.5 and 4.6. The independence of the value of the turbulent flux $\overline{w\theta}$ of the value of S_c is demonstrated in §4.7. Finally, some details of the skewness and kurtosis of the turbulent scalar and velocity fields are presented in §4.8.

4.1. *Flow visualization*

Longitudinal and lateral sections from LIF (figures 2*a*, *b*) show that the initially sharp interface – a material surface – is convoluted and displaced by the turbulence to a distance of $O(l_u)$ from the location of the mean interface defined by the $0.5\bar{C}$ concentration contour. The lengthscale, l_u, is derived from the autocorrelation of the longitudinal velocity signal, u, by utilizing Taylor's hypothesis, which is accepted to be valid for decaying grid-generated turbulence (i.e. $l_{R_{11(r,0,0)}}$). The perturbed interface shows a range of scales of deformation: l_u to l_{Kol} (typically at $x = 50$ cm, $l_u \sim 1.5$ cm, $l_{Kol} \sim 0.07$ cm). The sharp interface is not eroded, rather it is convoluted spatially, and the mean interface half-width, $\bar{h}$ (defined by $\Delta C/(\mathrm{d}C/\mathrm{d}z)$), as opposed to the instantaneous interface thickness, grows with increasing downstream distance from the grid in a manner similar to integral scales so that $\bar{h}/l_u$ is constant (see figures 6, 7). We estimate the instantaneous interface thickness, σ, to be of order $(2\kappa t)^{1/2}$ from molecular diffusion arguments. However, as the interface is being simultaneously folded, distorted and stretched, this estimate is probably an upper bound. In figure 2, the diffusivity of the dye is approximately equal to the mass diffusivity ($\sim 10^{-5}$ cm^2 s^{-1}) so that at $x = 50$ cm, $\sigma \sim 0.01$ cm. Note that the mean interface half-width, $\bar{h}$, need not, in general, be related to the integral lengthscale, even though $\bar{h}/l_u$ is constant. For example, for stationary homogeneous turbulence $\bar{h}$ will grow continuously in time even though the integral lengthscale remains constant. It should be understood that for decaying grid turbulence $\bar{h}/l_u \approx$ constant is a consequence of the growth of $\bar{h}$ and l_u.

Mixing is seen to comprise:

(i) coarse homogenization by entrainment (or engulfment) of scalar blobs $O(l_u)$ in size;

(ii) reduction of the scale of $O(l_u)$ blobs by breakup and deformation;

(iii) mixing by molecular diffusion which results from the greatly enhanced scalar gradients arising from the interleaving of material surfaces.

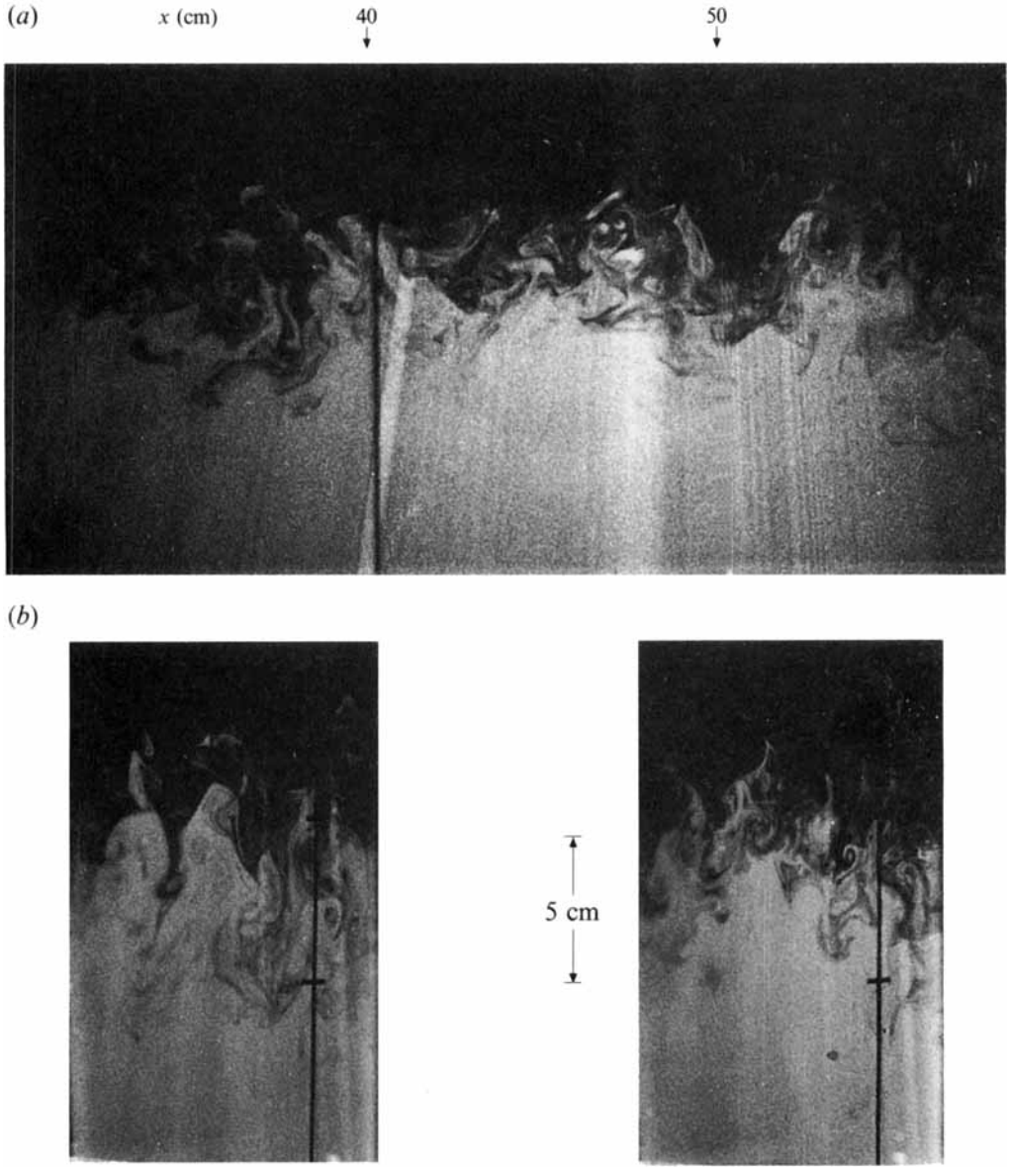

FIGURE 2. (*a*) Longitudinal section from LIF (x, z-plane). (Flow is from left to right, $\Delta\bar{\rho} = 0$ kg m^{-3}.) (*b*) Lateral sections from LIF (y, z-plane). $\Delta\bar{\rho} = 0$ kg m^{-3}, $x = 94$ cm. (Note that scales are distorted due to parallax.)

Mechanically, the process is one where gradients are increased until eventually limited by molecular diffusion. Whereas the scale of the major protuberances and depressions point to the main (i.e. integral or energy-containing) eddies of the turbulence as the agents of engulfment (Bevilaqua & Lykoudis 1977), the frequent occurrence of counter-rotating vortices, both above and below the interface, suggest that such structures may also play a role in the reduction of $O(l_u)$-size blobs. Such features are common in both longitudinal and lateral sections.

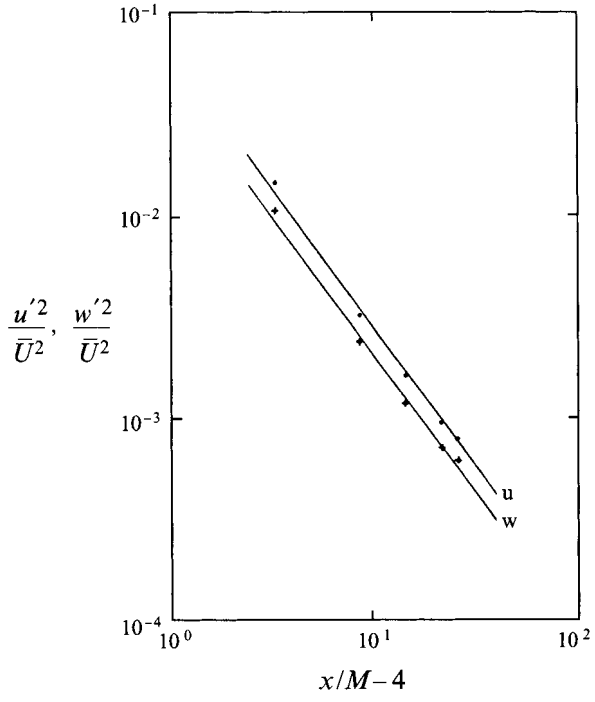

FIGURE 3. Decay of turbulent velocity fluctuations. The decay curves are of the form $(u_i'/U)^2 = A(x/M-4)^{-1.4}$ with $A = 0.07$, 0.05 for u', w' respectively.

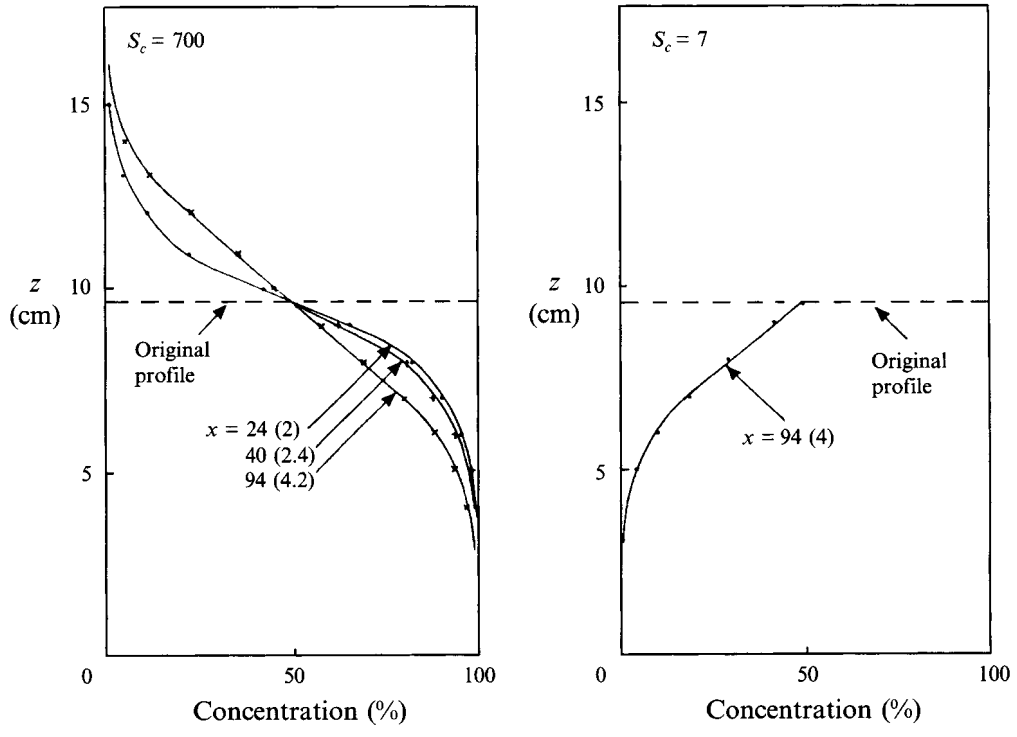

FIGURE 4. Mean scalar profiles ($S_c = 7$ and 700) at various downstream locations, x. The values of the interface half-width $\bar{h}$ are shown in parentheses.

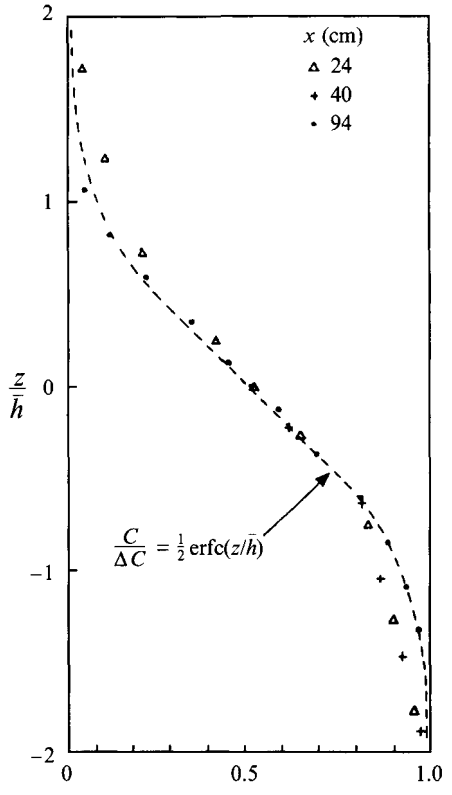

FIGURE 5. Self-similar evolution of mean scalar profiles for $S_c = 700$. Ordinate is non-dimensionalized by the mean interface thickness $\bar{h}$.

4.2. *Velocity field*

The decay of the turbulent velocity fluctuations from the grid for the passive scalar case (with salt/sugar, or heat as scalars) was determined to be identical to the homogeneous case (i.e. without any scalars). This is shown in figure 3. The decay curves are of the form $(u_i'/U)^2 = A(x/M-4)^{-1.4}$ with $A = 0.07, 0.05$ for u', w' respectively, in agreement with reported grid-turbulence data (e.g. Sreenivasan *et al.* 1980). The similarity of ϕ_w spectra of figure 12 for $S_c = 7$ and 700 shows that the scalars are truly passive, and that the associated velocity fields are not measurably different. A standard method to calculate the energy dissipation rate, ϵ, is to assume isotropy of the velocity field (Sirivat & Warhaft 1983). Thus the energy dissipation rate was found, from $\epsilon = (3/2)(\mathrm{d}/\mathrm{d}t)(u'^2)$, to be $0.147\,(\bar{U}^3/M)(x/m-4)^{-2.4}$, and this was used to determine the Kolmogorov lengthscale, l_{Kol}.

4.3. *Mean scalar profiles*

The evolution of the mean scalar profiles is shown in figure 4. The original two-layer profile is changed owing to the turbulent transport of mean scalar. The extent of the linear gradient of mean scalar at the centre of the interface grew with increasing downstream distance. The profile for $S_c = 7$ at $x = 94$ cm has the same (but inverted) form as the $S_c = 700$ profile at $x = 94$ cm. The mean scalar profiles, when normalized by the half-width, $\bar{h}$, of the interface, are found to be approximately self-similar (figure 5). It is seen that the degree of self-similarity improves with increasing distance from the turbulence-generating grid. The half-width, $\bar{h}$, determined by the intercept of the

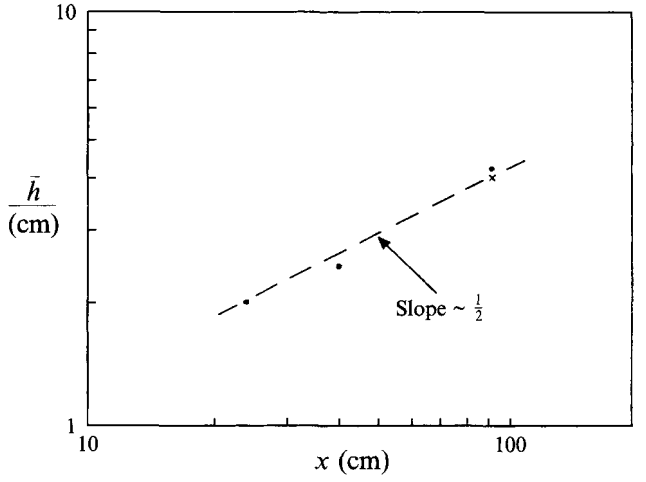

FIGURE 6. Evolution of mean interface half-width, $\bar{h}$. ($\times$, $S_c = 7$; and $\bullet$, 700).

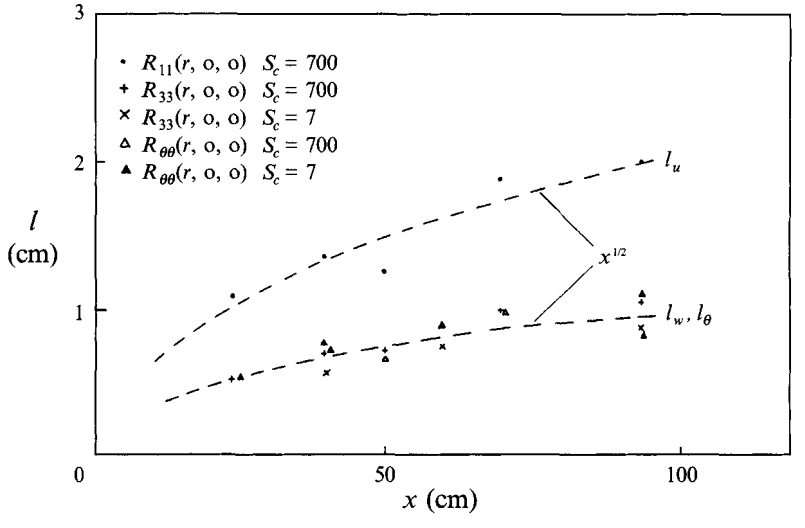

FIGURE 7. Evolution of integral lengthscales at centre of interface, $z = 0$, for $S_c = 7$ and 700. Dashed lines indicate an $x^{1/2}$ growth. Longitudinal, l_u, transverse, l_w, and scalar, l_θ, integral scales were determined from autocorrelation of u-, w- and θ-signals.

extrapolation of the central linear part of the mean scalar profile to the ordinate axis, i.e. $\Delta C/(\mathrm{d}C/\mathrm{d}z)_{z=0}$, is seen to grow as $x^{1/2}$ (figure 6). These results are in keeping with diffusion theory (Tennekes & Lumley 1982) which suggests that a constant value for the eddy diffusion coefficient K_t of the turbulent flow will give rise to an error function profile from an initial two-layer mean scalar profile. In decaying grid-generated turbulence, K_t is approximately constant since the direct effects of velocity decay are balanced by increases in Lagrangian length- and timescales (Batchelor & Townsend 1956; Tennekes & Lumley 1982).

4.4. *Lengthscales*

Figure 7 shows that integral lengthscales derived from the autocorrelation of the u, w and θ signals (longitudinal and lateral velocities, and scalar concentration) exhibit the approximate $x^{1/2}$ growth typical of grid turbulence (Tennekes & Lumley 1982). In

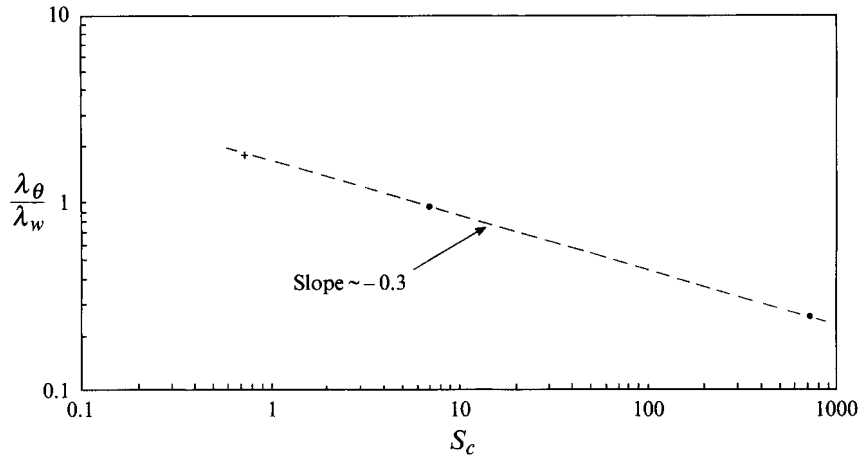

FIGURE 8. Variation of the ratio of scalar and velocity microscales with S_c at centre of mean interface, $z = 0$. Dashed line indicates a -0.3 power law. +, Keffer *et al.* (1977) data from wind tunnel experiments with heat as tracer, $x/M = 41$; ●, present data from water tunnel experiments with salt or heat as tracer, $x/M = 30$.

keeping with isotropic turbulence theory, the value of the longitudinal integral lengthscale is twice the value of the transverse integral lengthscale, i.e. $l_{R_{11(r,0,0)}} = 2l_{R_{33(r,0,0)}}$ (or $l_u = 2l_w$). It is seen that there is no effect of S_c on integral lengthscales. However, the scalar Taylor microscales of figure 8 show that $\lambda_{S_c=7} > 15\,\lambda_{S_c=700}$. The data of figure 8 show that the ratio $\lambda_\theta/\lambda_g \sim S_c^{-0.3}$ (where $\lambda_g = \lambda_w$ to abide by a conventional notation). Note that as the scalar field is dynamically passive, it is only the value of the scalar microscale λ_θ which varied. The wind-tunnel data ($P_r = 0.7$) of Keffer *et al.* (1977), at a similar value of x/M to the present experiments, albeit arising from a monoplane grid of horizontal bars, is in (surprising) agreement. The Taylor microscales were determined from a parabola fitted to the curve of the autocorrelation of the θ- and w-signals. This method only gave an approximate result for $S_c = 700$ owing to the limited spatial response of the conductivity probe. Thus the result $\lambda_\theta/\lambda_g \sim S_c^{-0.3}$ is likely to be an upper bound (i.e. the absolute value of the exponent of S_c is likely to be greater than 0.3). The variation of λ with S_c arises because with increasing S_c (or P_r), the scalar field is exposed to a more extensive spectrum of strain-rate fluctuations (see the spectra of figure 12), and there exist increasingly smaller blobs of scalar. Consequently it can be expected that the ratio λ_θ/λ_g will decrease with increasing S_c. For fully isotropic turbulence and scalar fields, Corrsin (1951) determined, analytically, that $\lambda_\theta/\lambda_g \sim P_r^{-0.5}$. Numerical simulations of Shirani, Ferziger & Reynolds (1981) showed both R_λ and P_r to be significant within the range considered ($2 < R_\lambda < 22$. $0.2 < P_r < 5$) in that λ_θ/λ_g varied approximately as $P_r^{-0.2}$, the ratio decreasing with R_λ for $P_r < 1$ but increasing with R_λ for $P_r > 1$.

The ratio, r, of the mechanical to thermal integral timescales (given by the ratio of the turnover times of the energy-containing velocity and scalar eddies) governs the evolution of the scalar and turbulent fields. The value of r depends on available production mechanisms because the 'energy containing eddies are influenced significantly by the production mechanisms of the respective velocity and scalar fields' (Newman, Launder & Lumley 1980). For uniformly heated decaying grid-generated turbulence, Sreenivasan *et al.* (1980) found that the ratio $l_{R_{\theta\theta(r,0,0)}}/l_{R_{11(r,0,0)}} = l_\theta/l_u = r$ maintained a constant value of 0.8 for $15 < x/M < 100$. When the thermal field was

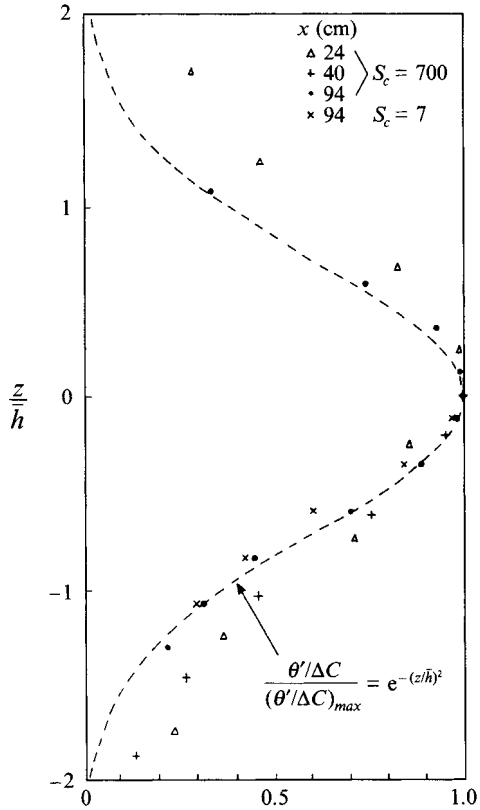

FIGURE 9. Self-similar evolution of scalar fluctuations for $S_c = 7$ and 700. Ordinate is non-dimensionalized by the interface thickness $\bar{h}$.

introduced at smaller scales by a fine heated screen (i.e. $M_\theta < M$) there was an asymptotic evolution, as the coupling increased, towards unity for r.

For the present experiments $M_\theta = M$ since the origins of the velocity and scalar fields are coincident; and, consistent with the preceding discussion, l_θ/l_u is found to be constant ($= 0.5$). Additionally, figure 7 shows that $l_{R_{\theta\theta}}$ is the same for $S_c = 7$ and 700, so that r is also independent of S_c (or P_r), even though it has been established that the ratio of the microscales, λ_θ/λ_q, is dependent upon S_c. This distinction between the integral scales and microscales is revealing; one implication is that the small scales and molecular effects are not significant in the engulfment process. As will be seen later (see §4.7 on fluxes), the fact that the flux is independent of molecular diffusivity is additional proof of the disparate effects on large and small scales.

4.5. *Scalar fluctuations*

For statistically stationary turbulence, the evolution equation for the scalar fluctuations, which describes the balance between turbulent and molecular transport, gradient production and molecular dissipation of $\overline{\theta^2}$, is given by Townsend (1976) as

$$\bar{U}_k \frac{\partial}{\partial x_k}(\tfrac{1}{2}\overline{\theta^2}) = -\frac{\partial}{\partial x_k}\left[\tfrac{1}{2}\overline{\theta^2 u_k} - \kappa \frac{\partial}{\partial x_k}(\tfrac{1}{2}\overline{\theta^2})\right] - \overline{\theta u_k}\frac{\partial C}{\partial x_k} - \overline{\kappa\left(\frac{\partial \theta}{\partial x_k}\right)^2}, \tag{1}$$

where $\boldsymbol{x} = (x, y, z)$ is a right-handed Cartesian coordinate system with z directed in the vertical, $\tilde{u} \equiv \bar{U}_i + u_i \equiv (u, v, w)$, κ is the species diffusivity, and passive scalar

quantities are mean, C, or fluctuation $\overline{\theta^2}$. Note that C and θ are dimensionless, and that $0 < C < 1$ by definition.

Examination of the evolution equation for $\overline{\theta^2}$ for the present stepwise mean scalar profile shows that the turbulent and molecular transport terms for $\overline{\theta^2}$ exist. This is unlike the linear passive scalar gradient case, where homogeneity in the direction of the gradient makes them vanish. Here, the inhomogeneity results in a balance between gradient production, dissipation and turbulent and molecular transport, compared with the simpler production/dissipation balance of the linear case.

The scalar fluctuations in the experiments (figure 9), like the mean scalar profiles, are approximately self-similar when normalized by the half-width, $\bar{h}$, of the interface and the local maximum value of $\theta'/\Delta C$, with the similarity improving with distance from the grid (recall Libby's 1975 analysis). However, the longitudinal evolution of $\theta'/\Delta C$, illustrated in figure 10 at the centreline of the interface, is found to be a weak function of S_c. Observed values of $\theta'/\Delta C$ grow from 0.22 at $x/M = 8$ to 0.28 at $x/M = 30$ for $S_c = 700$, and from 0.22 to 0.25 for $S_c = 7$. In comparison the consensus among heat-in-air experiments ($P_r = 0.7$) for this configuration is a near constant value of $\theta'/\Delta C = 0.22$, as the experiments of Watt & Baines (1973), Keffer *et al.* (1977), and LaRue *et al.* (1981) show. (Note that values of $\theta'/\Delta C$ for $S_c = 700$ are likely to be an underestimate owing to the limited spatial resolution of the conductivity probe.) The scalar equation for $\overline{\theta^2}$ (equation (1)) simplifies for the present configuration to

$$\bar{U}\frac{\partial}{\partial x}\overline{\theta^2} = -2\overline{\theta w}\frac{\partial C}{\partial z} - 2\kappa\frac{\overline{\partial\theta}}{\partial x_i}\frac{\overline{\partial\theta}}{\partial x_i} - \frac{\partial}{\partial z}\overline{(w\theta^2)} + \kappa\frac{\partial^2\overline{\theta^2}}{\partial z^2}. \tag{2}$$

This shows that the evolution of $\overline{\theta^2}$ is determined by the balance of mean gradient production, dissipation, turbulent and molecular transport respectively. Order-of-magnitude analysis is facilitated by the usual simplifications:

$$2\kappa\frac{\overline{\partial\theta}}{\partial x_i}\frac{\overline{\partial\theta}}{\partial x_i} \approx 6\kappa\frac{\overline{\theta^2}}{\lambda^2}, \tag{3}$$

$$\overline{w\theta^2} \approx (u' l_w)\frac{\delta\overline{\theta^2}}{\delta z}. \tag{4}$$

Substitution of data for $S_c = 7$ at $x = 94$ cm ($l_w = 1$ cm, $u' = 0.23$ cm s^{-1}, $\lambda = 0.5$ cm, $\kappa = 0.0014$ cm^2 s^{-1}, $\overline{\theta^2} = 0.07$, $\delta z \approx \bar{h} \approx 2$ cm) shows that the molecular transport term is approximately a thousand times smaller than the gradient production, dissipation and turbulent transport terms. Thus the difference in the values of θ' with downstream distance between $S_c = 7$ and 700, can be attributed to the effect of the dissipation term $\kappa(\partial\bar{\theta}/\partial x_i)(\partial\bar{\theta}/\partial x_i)$, as the mean gradient profiles (§4.3) and the flux θw (see §4.7) are independent of the molecular diffusivity, K, of the scalar; and at the centre of the interface the value of the turbulent transport term $(\partial/\partial z)(\overline{w\theta^2})$ is zero. This influence of the molecular dissipation term, rather than the adjustment of the virtual origin to $-30M$ of LaRue *et al.* (1981), is the explanation for the discrepancy of the magnitude of $\theta'/\Delta C$ between the predictions of Libby (1975) and the experimental results (all at $P_r = 0.7$) of Watt & Baines (1973), Keffer *et al.* (1977), and LaRue *et al.* (1981).

Increasing scalar diffusivity would produce more molecular mixing and result in a more uniform mixture at any given time. Danckwerts (1953) has defined the approach to uniformity by the intensity of segregation, I_s,

$$I_s = \frac{\theta'^2}{C(C_{max} - C)}. \tag{5}$$

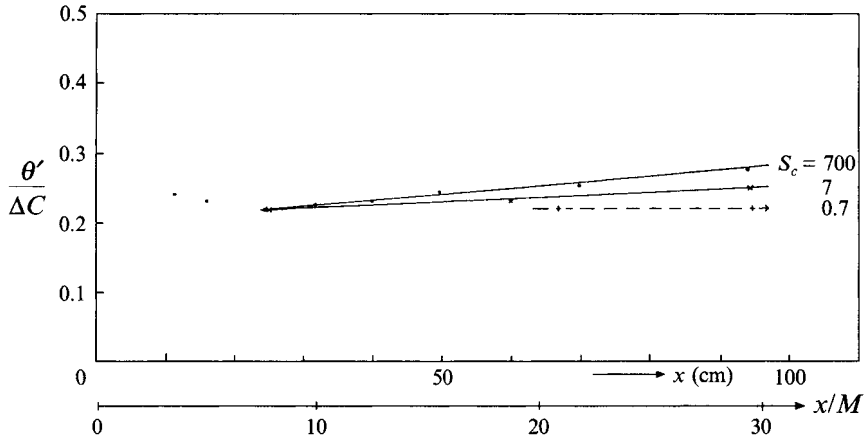

FIGURE 10. Effects of S_c on the evolution of normalized scalar fluctuation $\theta'/\Delta C$ at centre of mean interface, $z = 0$. Value of $\theta'/\Delta C$ for wind tunnel data ($S_c = 0.7$) is an approximately constant value of 0.22 for x/M values up to 180 (LaRue & Libby 1981).

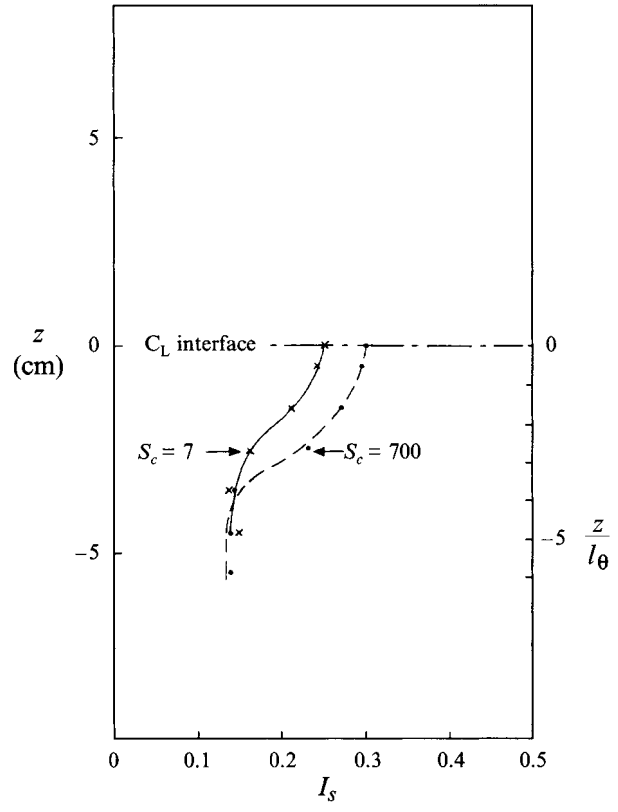

FIGURE 11. Variation of the intensity of segregation I_s (see equation (5)) with S_c for $S_c = 7$ and 700 at $x = 94$ cm. Note dimensional and non-dimensional ordinate scales. Right-hand ordinate is non-dimensionalized by the scalar integral scale l_θ (l_θ from autocorrelation of scalar signal). By definition $I_s = 0$ for a uniform mixture, and $I_s = 1$ in the absence of molecular mixing.

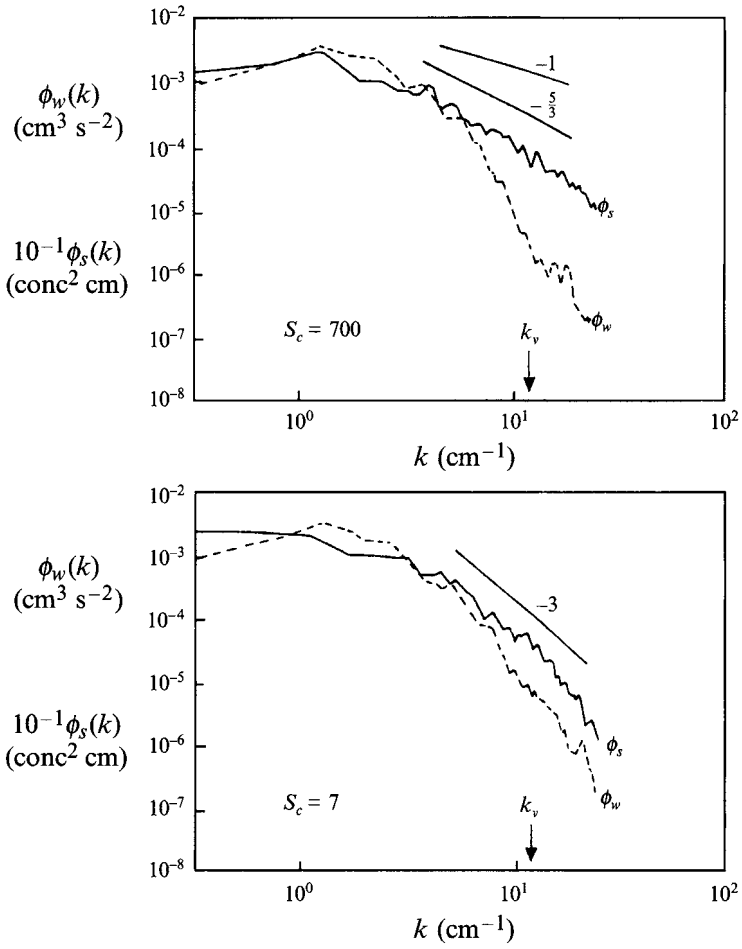

FIGURE 12. One-dimensional velocity (ϕ_w) and scalar spectra (ϕ_s) at centre of mean interface, $z = 0$, $x = 60$ cm, for $S_c = 7$ and 700. Also indicated are -1, $-\frac{5}{3}$ and -3 power law slopes. k_v indicates the Kolmogorov scale.

I_s varies between zero for a truly uniform mixture, and unity for a mixture without molecular mixing by definition. The effect of S_c on the uniformity is shown in figure 11, where the more diffusive scalar ($S_c = 7$) possesses a lower value of I_s at the interface and approaches uniformity more rapidly, e.g. $I_s = 0.175$ at $z/l_\theta \approx 2$ for $S_c = 7$ compared with $I_s = 0.175$ at $x/l_\theta \approx 3$ for $S_c = 700$ where l_θ is determined from autocorrelation of the scalar signal (see figure 7).

The present results are in accord with those of Koochesfahani & Dimotakis (1986) who, for a shear layer using chemically reacting scalars (see Breidenthal 1981), found that 'comparisons of liquid ($S_c = 600$) and gas phase ($S_c = 0.8$) data show that the normalized amount of chemical product formed in the liquid layer at high Reynolds number is 50% less than the corresponding quantity measured in the gas phase case'. Consequently, though the differences in θ' for varying S_c are small, they are not insignificant. The implications for reactions, in particular the more rapid approach to a homogeneous mixture for low S_c, are of significance for the chemical industry.

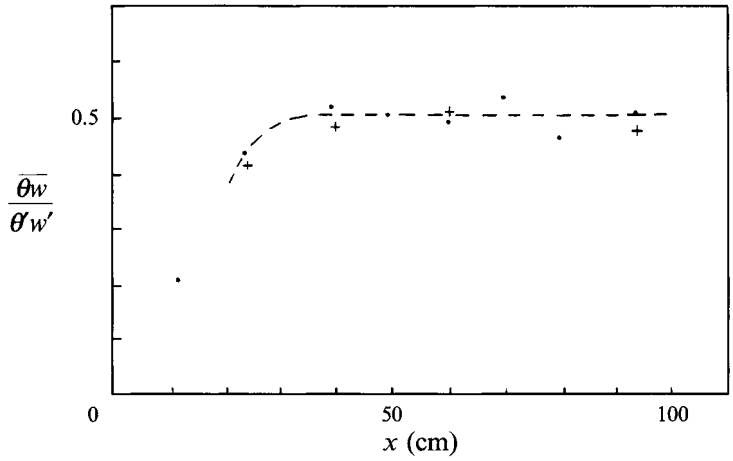

FIGURE 13. Evolution of normalized flux $\overline{\theta w}/\theta' w'$ at centre of mean interface $z = 0$ for $S_c = 7$ (+) and 700 (●). The value of the normalized flux is constant for large values of x.

4.6. *Spectra*

Spectra of the velocity and scalar fields for $S_c = 7$ and 700 are shown in figure 12. As noted earlier, the similarity of ϕ_w for $S_c = 7$ and 700 shows that the scalars are passive. The forms of the scalar spectra ϕ are seen to be dependent on S_c. For $S_c = 700$, the slope of the scalar spectra is seen to be approximately $-\frac{5}{3}$, whereas for $S_c = 7$, the slope is approximately -3. For large S_c ($\gg 1$), Batchelor (1959) determined that in the viscous-convective subrange (i.e. $k > (\epsilon/\nu^3)^{1/4}$) the scalar spectrum extends much further into the high-wavenumber range, owing to the difference in the diffusivities ν and κ. The spectral density would depend only on the spectral flux of scalar variance, $\epsilon_s(\theta^2/s)$ and on the strain rate $\gamma(s^{-1})$ since diffusivity is important only beyond this subrange. Accordingly, dimensionally $F(k) \sim (\epsilon_s/\gamma)k^{-1}$. The finite-probe resolution of the conductivity probe does not allow this to be tested satisfactorily.

For low P_r (or S_c) < 1, the strain rate γ is irrelevant because the scalar blobs are larger than the scales of uniform strain, so that the mechanism of alignment and compression of scalar wavecrests characteristic of $S_c \gg 1$ is inoperable. Rather, the spectral density is essentially a balance between the production of small-scale scalar fluctuations by distortion of the local mean gradient by the turbulence and the diffusive suppression of these fluctuations. Batchelor, Howells & Townsend (1959) found $F(k) \sim k^{-17/3}$. As noted in figure 8, the scalar microscale was found to vary with S_c: this arises simply from the more extensive spectrum for large S_c. Evidently (figure 12) for large S_c more of the dissipation of scalar occurs at scales much smaller than the Kolmogorov scale $k_\nu^{-1} = (\nu^3/\epsilon)^{1/4}$, so that the scalar field is exposed to the entire spectrum of strain rate fluctuations with the result that scalar and velocity microscales are distinct.

4.7. *Fluxes*

Figure 13 shows that measured values of the normalized flux at the centreline of the interface are constant and independent of the value of S_c. The observation that F is independent of molecular diffusivity indicates that large-scale activity, which is relatively unaffected by molecular diffusivity, is dominant in the engulfment process. Values of the normalized flux, F, decreased with distance from the centre of the interface ($z/\bar{h} = 0$), and the vertical distribution of F was approximately self-similar

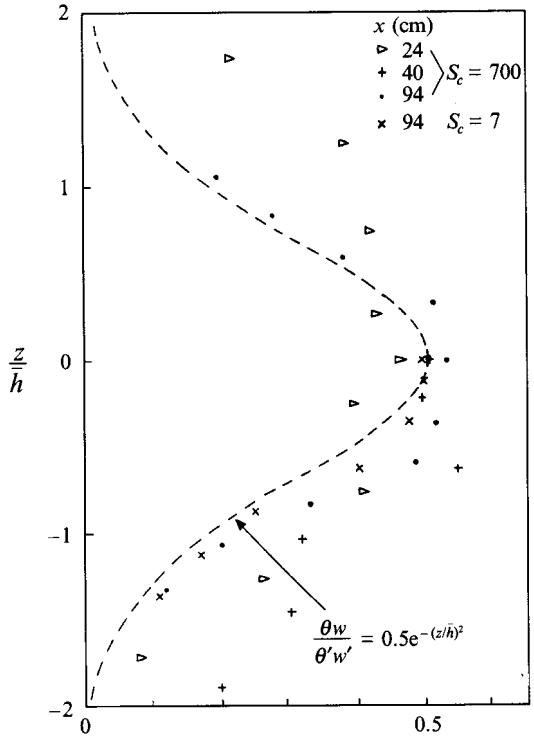

FIGURE 14. Approximate self-similar evolution of normalized flux $\overline{\theta w}/\theta' w'$ for $S_c = 7$ and 700. Ordinate is non-dimensionalized by the interface thickness $\bar{h}$.

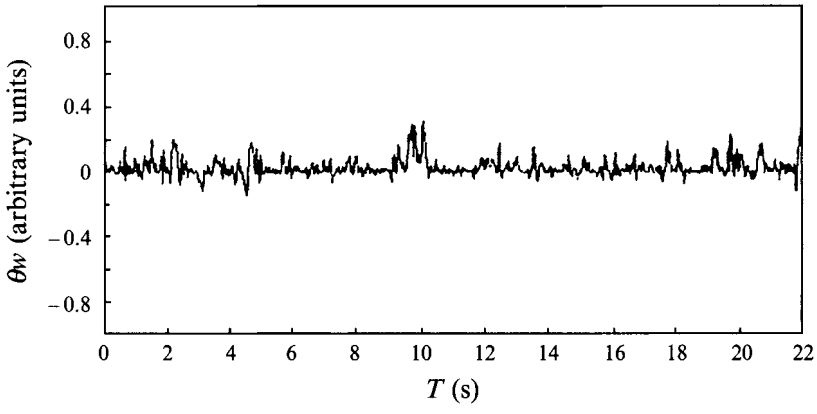

FIGURE 15. Time series of θw at centre of interface showing intermittency of engulfing events. Data at $x = 60$ cm.

though the scatter was considerable (figure 14). The scatter is due not only to correlating and dividing small quantities but also to the reduction in the fraction of eddies that are tagged by the scalar away from the interface.

The time series of instantaneous θw shows that it is intermittent (figure 15), both temporally and spatially (since the levels of turbulence intensities are weak and Taylor's hypothesis is valid). The frequency of the intermittent peaks in the θw time

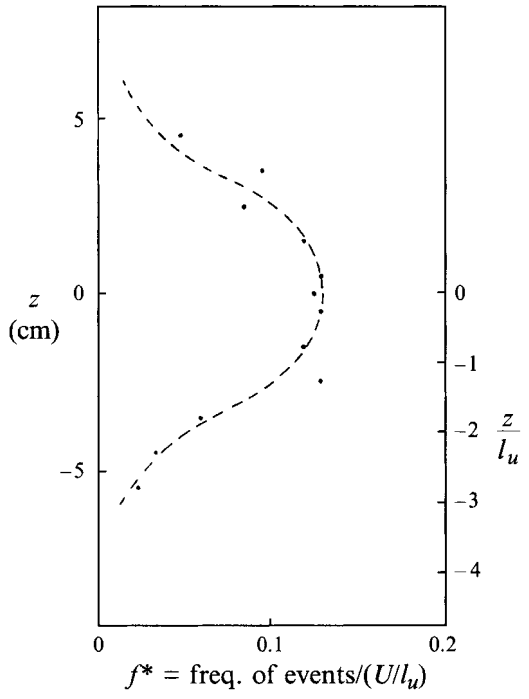

FIGURE 16. Vertical distribution of non-dimensionalized frequency of engulfing events f^*. Note dimensional and dimensionless ordinate scales. Right-hand ordinate is non-dimensionalized by the velocity integral scale l_u. Data at $x = 94$ cm; $S_c = 700$.

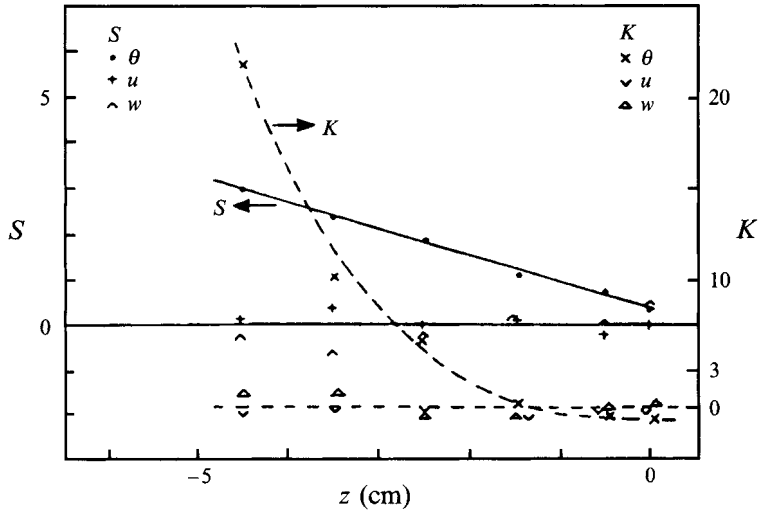

FIGURE 17. Skewness, S, and kurtosis, K, of u, w and θ. Note that ordinate scale at left is for skewness, and ordinate scale at right is for kurtosis. Data at $x = 60$ cm; $S_c = 700$.

series was determined using an empirically determined threshold. (The value of the threshold which changed the number of events least was found to be 0.35 of the maximum value of θw in the time series.) The frequency of the intermittent peaks in the θw time series (physically the frequency of individual engulfing events) is low – that is

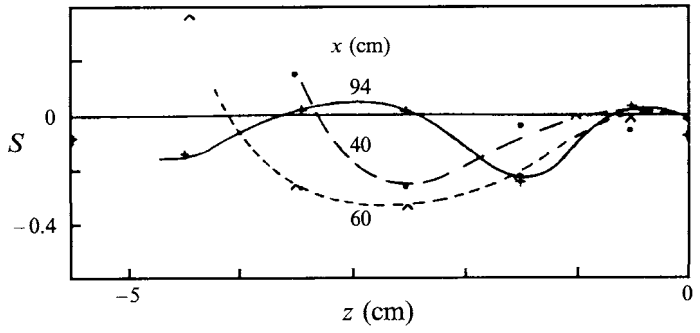

FIGURE 18. Variation of skewness of derivative of θ away from centre of interface. Data at $x = 40$, 60, 94 cm, $S_c = 700$.

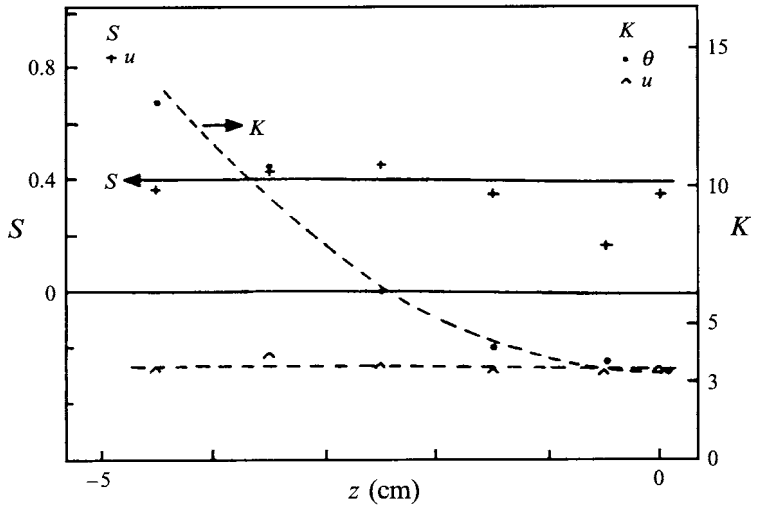

FIGURE 19. Skewness and kurtosis of derivative of u and θ. Note that ordinate scale at left is for skewness, and ordinate scale at right is for kurtosis. Data at $x = 60$ cm; $S_c = 700$.

to say that the occurrence of engulfing events is rare. The maximum value of f^*, the aforementioned frequency non-dimensionalized by the mean velocity and integral length, $\bar{U}/l_u$, is about 0.1. The similar forms of the vertical distributions of f^* and F (see figure 16) suggest that the principal factor determining F (i.e. the flux or average engulfment rate) is the frequency of events, rather than differences in the intensities (or distribution) of such events.

4.8. *Statistical and geometrical features of scalar and velocity fields*

The skewness and kurtosis of the u- and w-signals possess near Gaussian values. The scalar signal (θ), however, is never Gaussian and particularly away from the centreline of the interface the intermittency of the flapping interface is as shown in figure 17. This finding is in agreement with the observations of Venkataramani & Chevray (1978) who found that the scalar signal was skewed in the presence of a vertical linear gradient of passive scalar, even though u, w were Gaussian. (For the case without a mean scalar gradient, Yeh 1971 and Yeh & Van Atta 1973 found that the velocity and scalar signals were Gaussian.)

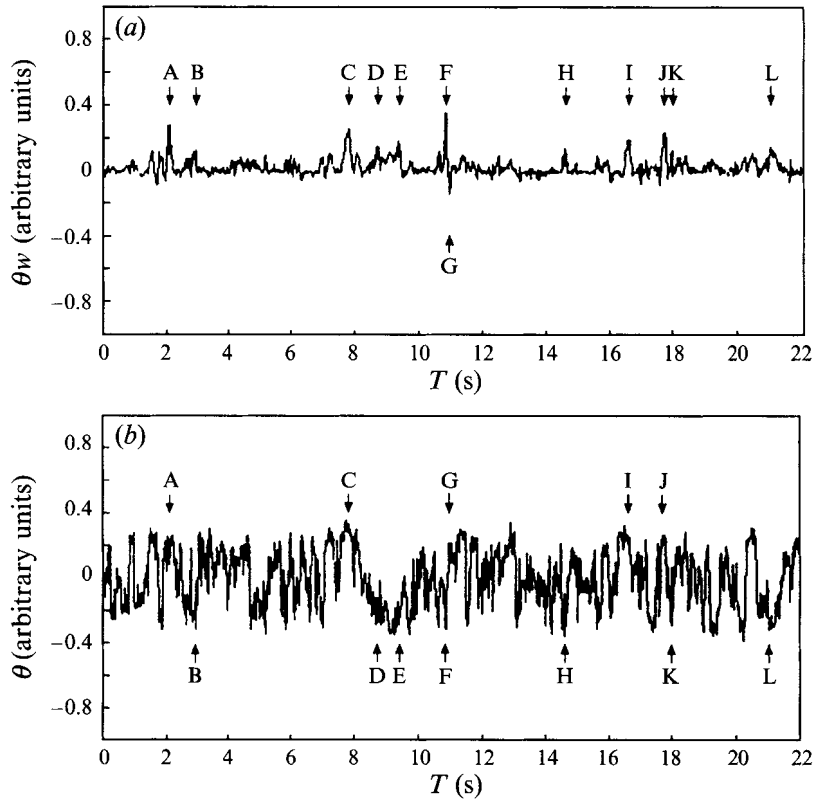

FIGURE 20(*a*, *b*). For caption see facing page.

The higher-order statistics for the derivative are traditionally used to infer the degree of homogeneity of the small scales (e.g. Batchelor 1953). However, a geometrical interpretation may be inferred; for example, Sreenivasan *et al.* (1980) concluded that the skewness of the derivative of the scalar signal $S_{\theta_{x_1}}$ is non-zero only when the mean velocity and mean scalar gradients are both non-zero,

$$\operatorname{sgn}(S_{\theta_{x_1}}) = -\operatorname{sgn}\left(\frac{\partial \bar{U}}{\partial x_2}\right) \operatorname{sgn}\left(\frac{\partial C}{\partial x_2}\right). \tag{6}$$

By considering the translation of an eddy through a linear gradient of a passive scalar however, Budwig *et al.* (1985) showed that

$$-\operatorname{sgn}(S_{\theta_{x_i}}) = \operatorname{sgn}\overline{\left(\frac{\partial \theta}{\partial x_i}\right)^3} \Big/ \left(\overline{\left(\frac{\partial \theta}{\partial x_i}\right)^2}\right)^{3/2} = \operatorname{sgn}\left(\frac{\partial C}{\partial x_i}\right) \quad \text{(no sum on } i\text{)}, \tag{7}$$

where, as usual, C is the mean and θ is the scalar fluctuation. This is demonstrated in figure 18: at the interface centreline, where $\mathrm{d}C/\mathrm{d}x = 0$ (the mean concentration being always 50% of ΔC between the layers) the skewness of the derivative is zero. Conversely, below the interface, where there is a longitudinal scalar gradient, the skewness is non-zero. (Antonia *et al.* 1978 found that $S_{\theta_{x_i}} \approx 0$ for the zero gradient case of a uniformly heated grid.) Figure 19 shows that the present value for $S_{u_{x_i}}$ of 0.4 (with $R_\lambda \sim 12$) is in good agreement with the data of figure 6.3 of Batchelor (1953); and as for the scalar signal, the intermittency of the flapping interface is evident in the derivative of the scalar signal away from the interface.

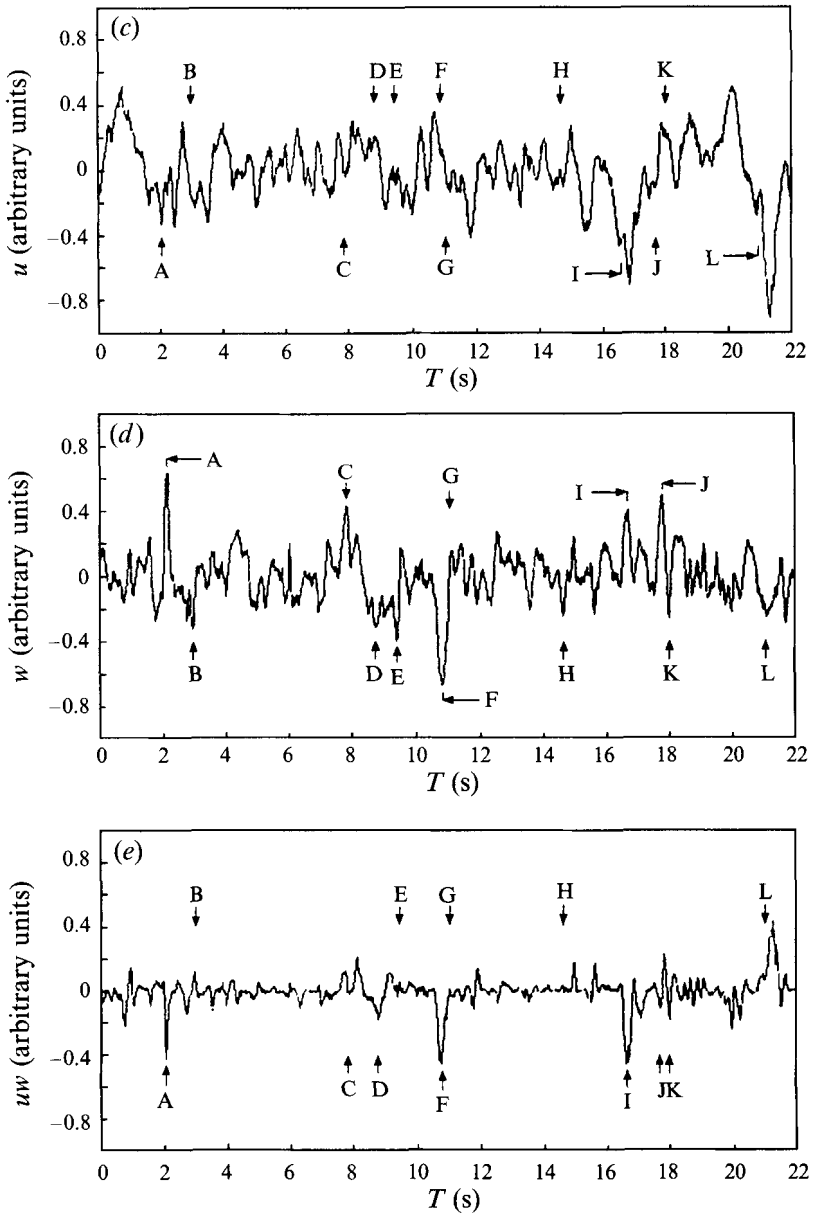

FIGURE 20. Time series of θw, θ, u, w, uw at centre of mean interface, $S_c = 700$. A–L mark events of significant θw transport. Data at $x = 94$ cm. (*a*) θw; (*b*) θ; (*c*) u; (*d*) w; (*e*) uw time series.

The detailed examination of the instantaneous scalar and velocity fields at the principal locations of engulfment, using θw as the indicator signal, is revealing (figure 20). For large values of θw, both θ and w must be large on average. However, it is not obvious that the values of θ and w should be extrema, which is seen to be the case for both θ and w (figure 20*b*, *d*). Figure 20(*b*, *d*) also shows that minima and maxima of θ and w are likely to occur with an approximately equal likelihood. It is also evident from figure 20(*e*) that peak values of uw are correlated with θw events, though again it is not obvious why there should be a correlation for this flow of shear-free grid-generated turbulence. The agreement is not complete, as only events A, F, I, B, D, J,

K (i.e. seven out of a total of 12 events) are extrema of the instantaneous Reynolds stress uw. Figure 20 is a spanwise plane view of the flow (i.e. the x, z plane) so that θw events associated with eddies both perpendicular and parallel to the plane are detected, whereas only Reynolds stress extrema from the vorticity perpendicular to the spanwise plane are found by the present arrangement. Thus the number of uw extrema associated with θw extrema may be expected to be one half the number of θw extrema, which is approximately the case. It is likely that the correlation between θw events and instantaneous Reynolds stress extrema would have been more complete if measurements of vw correlations were available.

It is speculated that the above correlations suggest the kinematic interpretation that θw events arise from random horizontal translations of eddies. Eddies whose vorticity resides in a horizontal plane will not experience a vertical force due to a horizontal translation as $\rho u \times \omega_z = 0$, where u is the horizontal component of the turbulent velocity vector (u, v, w), and ω_z is the vorticity component parallel to the z-axis of the vorticity vector $(\omega_x, \omega_y, \omega_z)$. Eddies whose vorticity axes are parallel to the x- and y-axes when subjected to a horizontal translation will experience a vertical force as $\rho u \times \omega_x \neq 0$ and $\rho u \times \omega_y \neq 0$. This is due to the Magnus effect where a non-zero vorticity–velocity cross-product generates a body force (see Tennekes & Lumley 1982). This kinematic interpretation suggests a correlation between θw events and Reynolds stress extrema uw and vw. The present experiments involve single-point measurements; experiments with arrays of probes would offer further insight into the kinematics of mixing.

5. Summary and conclusions

Experiments were undertaken to examine the nature of mixing of passive scalars in a two-layer scalar profile due to shear-free decaying grid-generated turbulence in a water tunnel. Heat and salt ($S_c = 7$ and 700 respectively) were used as scalars so that comparison with wind-tunnel ($S_c = P_r = 0.7$) results distinguishes the effect of molecular diffusivity.

The downstream evolution of the mean concentration, scalar fluctuation and flux ($\overline{\theta w}/\theta' w'$) profiles are approximately self-similar. Values of the integral lengthscales for the longitudinal and lateral velocities and scalar concentrations were found to be independent of S_c, unlike the Taylor microscales which vary as $\lambda_\theta/\lambda_g \sim S_c^{-0.3}$, thus illustrating the disparate effects of diffusivity on large and small scales. The scalar variance θ' increases with distance for large S_c (> 100). Scalar spectra vary with S_c, with approximate observed slopes of $-\frac{5}{3}$ for $S_c = 700$ and -3 for $S_C = 7$ for wavenumbers up to approximately $(0.5k_v)^{-1}$. The value of the time-averaged scalar flux $\overline{\theta w}$ is independent of the value of S_c. Time series show that θw is intermittent. They also show that the frequency of intermittent events (physically the frequency of engulfing events), non-dimensionalized by the mean velocity and integral length, is about 0.1, which demonstrates the rarity of engulfing events. Visualizations show that mixing comprises engulfment of 'blobs' with scales of the order of the integral scale l_u with subsequent reduction by breakup and deformation. Analysis of the time series for θw and uw reveals that there is a correspondence between locations of engulfment and Reynolds stress extrema. They also show that the magnitude of the time-averaged flux $\overline{\theta w}$ depends on the frequency, rather than variations in the amplitude, of θw events.

REFERENCES

ALEXOPOULOS, C. C. & KEFFER, J. F. 1971 Turbulent wake in a passively stratified field. *Phys. Fluids* **14**, 216–224.

ANTONIA, R. A., CHAMBERS, A. J., VAN ATTA, C. W., FRIEHE, C. A. & HELLAND, K. N. 1978 Skewness of temperature derivative in a heated grid flow. *Phys. Fluids* **21**, 509–510.

BATCHELOR, G. K. 1953 *The Theory of Homogeneous Turbulence.* Cambridge University Press.

BATCHELOR, G. K. 1959 Small-scale variation of convected quantities like temperature in turbulent fluid. Part 1. General discussion and the case of small conductivity. *J. Fluid Mech.* **5**, 113–133.

BATCHELOR, G. K., HOWELLS, I. D. & TOWNSEND, A. A. 1959 Small-scale variation of convected quantities like temperature in turbulent fluid. Part 2. The case of large conductivity. *J. Fluid Mech.* **5**, 134–139.

BATCHELOR, G. K. & TOWNSEND, A. A. 1956 Turbulent diffusion. In *Surveys in Mechanics* (ed. G. K. Batchelor & R. M. Davis). Cambridge University Press.

BEVILAQUA, P. M. & LYKOUDIS, P. S. 1977 Some observations on the mechanism of entrainment. *AIAA J.* **15**, 1194–1196.

BIDOKHTI, A. & BRITTER, R. E. 1987 Development of a stratified shear flow facility. Report to Topexpress Ltd., UK.

BRADSHAW, P. 1971 *An Introduction to Turbulence and Its Measurement.* Pergamon.

BREIDENTHAL, R. E. 1981 Structure in turbulent mixing layers and wakes using a chemical reaction. *J. Fluid Mech.* **109**, 1–24.

BUDWIG, R., TAVOULARIS, S. & CORRSIN, S. 1985 Temperature fluctuations and heat flux in grid-generated isotropic turbulence with streamwise and transverse mean-temperature gradient. *J. Fluid Mech.* **153**, 441–460.

CHAMPAGNE, F. H. & SLEICHER, C. A. 1967 Turbulence measurements with inclined hot wires. *J. Fluid Mech.* **28**, 177–182.

CORRSIN, S. 1951 The decay of isotropic temperature fluctuations in an isotropic turbulence. *J. Aeronaut. Sci.* **18**, 417–423.

DANCKWERTS, P. V. 1953 The definition and measurement of some characteristics of mixtures. *Appl. Sci. Res.* A **3**, 279–296.

DIMOTAKIS, P. E. 1987 Turbulent shear layer mixing with fast chemical reactions. *GALCIT Rep.* FM87-1.

HUQ, P. 1990 Turbulence and mixing in stratified fluids. PhD Dissertation, University of Cambridge.

JONES, W. P. & MUSONGE, P. 1988 Closure of the Reynolds stress and scalar flux equations. *Phys. Fluids* **31**, 3589–3604.

KEFFER, J. F., OLSEN, G. J. & KAWALL, J. G. 1977 Intermittency in a thermal mixing layer. *J. Fluid Mech.* **79**, 595–607.

KOOCHESFAHANI, M. M. & DIMOTAKIS, P. E. 1986 Mixing and chemical reactions in a turbulent liquid mixing layer. *J. Fluid Mech.* **170**, 83–122.

LARUE, J. C. & LIBBY, P. A. 1981 Thermal mixing layer downstream of a half-heated turbulence grid. *Phys. Fluids* **24**, 597–603.

LARUE, J. C., LIBBY, P. A. & SESHADRI, D. V. R. 1981 Further results on the thermal mixing layer downstream of a turbulence grid. In *3rd Symp. on Turbulent Shear Flows, Davis.*

LAWSON, R. E. & BRITTER, R. E. 1983 A note on the measurements of transverse velocity fluctuations with heated cylindrical sensors at small mean velocities. *J. Phys.* E: *Sci. Instrum.* **16**, 563–567.

LIBBY, P. A. 1975 Diffusion of heat downstream of a turbulence grid. *Acta Astronautica* **2**, 867–878.

LIN, C. C. (ed.) 1959 *High Speed Aerodynamics and Jet Propulsion Series*, vol. 5. Princeton University Press.

MACINNES, J. M. 1985 Numerical simulation of the thermal turbulent mixing layer. *Phys. Fluids* **28**, 1013–1014.

NEWMAN, G., LAUNDER, B. E. & LUMLEY, J. L. 1980 Modelling the behaviour of homogeneous scalar turbulence. *J. Fluid Mech.* **111**, 217–232.

SHIRANI, E., FERZIGER, J. H. & REYNOLDS, W. C. 1981 Mixing of a passive scalar in isotropic and sheared homogeneous turbulence. *Stanford Thermosci. Div. Tech. Rep.* TF-15.

SIRIVAT, A. & WARHAFT, Z. 1983 The effect of passive cross-stream temperature gradient on the evolution of temperature variance and heat flux in grid turbulence. *J. Fluid Mech.* **128**, 323–346.

SREENIVASAN, K. R., TAVOULARIS, S., HENRY, R. & CORRSIN, S. 1980 Temperature fluctuations and scales in grid-generated turbulence. *J. Fluid Mech.* **100**, 597–621.

TAYLOR, G. I. 1921 Diffusion by continuous movements. *Proc. Lond. Math. Soc.* **20**, 196–212.

TENNEKES, H. & LUMLEY, J. L. 1982 *A First Course in Turbulence*, 2nd Edn. MIT Press.

TOWNSEND, A. A. 1976 *The Structure of Turbulent Shear Flow*, 2nd Edn. Cambridge University Press.

VENKATARAMANI, K. S. & CHEVRAY, R. 1978 Statistical features of heat transfer in grid-generated turbulence: constant-gradient case. *J. Fluid Mech.* **86**, 513–543.

WARHAFT, Z. & LUMLEY, J. L. 1978 An experimental study of the decay of temperature fluctuations in grid-generated turbulence. *J. Fluid Mech.* **88**, 659–684.

WATT, W. E. & BAINES, W. D. 1973 The turbulent temperature mixing layer. *J. Hydr. Res.* **11**, 157–166.

WISKIND, H. K. 1962 A uniform gradient turbulent transport experiment. *J. Geophys. Res.* **67**, 3033–3048.

YEH, T. 1971 Scalar spectral transfer and higher order correlations of velocity and temperature fluctuations in heated grid turbulence. PhD dissertation, University of California (San Diego).

YEH, T. & VAN ATTA, C. W. 1973 Spectral transfer of scalar and velocity fields in heated-grid turbulence. *J. Fluid Mech.* **58**, 233–261.